High Voltage

WILEY

国家电网 STATE GRID 中国电力科学研究院有限公司 CHINA ELECTRIC POWER RESEARCH INSTITUTE | IET The Institution of Engineering and Technology

ORIGINAL RESEARCH OPEN ACCESS

Lightning-Induced Overvoltage on Overhead Distribution Line via Hybrid MTL-PEEC Method

Runyu Fu[1] | Jinxin Cao[1] | Yating Zhao[1] | Jianguo Wang[1] | Yaping Du[2] | Li Cai[1] | Mi Zhou[1] | Yuxuan Ding[2]

[1]The Engineering Research Center of Ministry of Education for Lightning Protection and Grounding Technology, School of Electrical Engineering and Automation, Wuhan University, Wuhan, China | [2]The Department of Building Services Engineering, the Hong Kong Polytechnic University, Hung Hom, Hong Kong, China

Correspondence: Jinxin Cao (jinxin.cao@connect.polyu.hk) | Jianguo Wang (wjg@whu.edu.cn)

Received: 12 January 2024 | **Revised:** 25 July 2024 | **Accepted:** 20 August 2024

Associate Editor: Amedeo Andreotti

ABSTRACT

Transient simulation are more economical and adaptable means of studying lightning overvoltage for overhead distribution line system compared to experiments. A hybrid multi-transmission-line (MTL)-partial element equivalent circuit (PEEC) method proposed for lightning-induced electromagnetic pulse (LEMP) simulation is verified using the rocket-triggered experimental results under a more complex line configuration for the first time. This method can improve computational efficiency while ensuring calculation accuracy. The agreement between experimental and simulation results further validates the adaptability and accuracy of the proposed method, which is adopted to calculate the LEMP on the extended double-circuit parallel unequal length line. The effects of various factors, such as the strike-point location, the amplitude and waveform of the lightning current, the line shape and length on the amplitude of overvoltage and pole flashover along the line are discussed. For double-circuit distribution lines, when lightning strikes the ground in front of centre of circuit I, the three-phase voltage waveforms are similar, all of which are negative or bipolar oscillation waves. The closer the lightning strike point is to the line, the greater the amplitude of the lightning current, and the voltage waveform develops towards a bipolar waveform, but the main peak remains negative. As the amplitude of lightning current increases, the maximum lightning-induced voltage amplitude along the line increases. The LEMP caused by the subsequent return-stroke current is always greater than that caused by the first return-stroke current. When the grounding resistance increases, the maximum voltage peak amplitude along the line remains unchanged.

1 | Introduction

The safe operation of the overhead distribution line system, an important component of the power system, directly affects the stability of the power grid and the reliability of power supply to users [1, 2]. The lightning overvoltage experienced by distribution lines mainly includes direct lightning overvoltage and lightning-induced overvoltage. Lightning-induced overvoltage refers to the discharge of lightning strikes on the ground or other buildings near the line, causing lightning-induced overvoltage or overcurrent on the distribution line through electromagnetic coupling [3–5]. Compared to transmission lines, the insulation level and voltage level of distribution systems are relatively low, and lightning poses a great threat to them, which may lead to issues such as insulator flashover, damage to surge arresters and reduced power quality. These issues will seriously affect the reliability and stability of electricity consumption. As have been reported, lightning-induced overvoltage causing over

90% of distribution line failures in areas with severe thunderstorms [6, 7].

At present, the existing widely used simulation methods for large-scale overhead transmission line systems are the numerical methods combined with circuit-based models. Circuit-based models can be smoothly integrated into commercial software, such as electro-magnetic transient programme (EMTP) and power systems computer-aided design (PSCAD) [8–10]. However, this circuit-based method cannot fully describe the impact of surge corona, grounding grid and lightning channels, and it does not consider the multiple coupling between iron towers, lighting channels and transmission lines. The lightning channel has a significant impact on the surge response of the struck tower. Ignoring the coupling from the channel to the tower will reduce the risk of lightning strikes [11, 12]. Due to its low voltage level, the calculation of induced lightning overvoltage in distribution lines must consider the coupling effect between the line and the lightning channel. Therefore, the calculation of induced lightning overvoltage in overhead distribution lines usually uses numerical calculation methods combining line-to-field coupling models [13, 14].

The widely used lightning transient analysis numerical calculation methods currently include full-wave numerical, hybrid electromagnetic and multi-conductor transmission line (MTL) methods [15–18]. These methods cannot achieve a good balance between computational accuracy and efficiency when modelling the complex power-line system for lightning-induced electromagnetic pulse (LEMP) simulation. Therefore, it is necessary to find a numerical method that can balance the simulation performance. The modelling of various components of overhead transmission lines includes modelling methods for short lines (partial element equivalent circuit [PEEC] method) [19–22] and modelling methods for long lines (MTL) [1]. Although considering the performance of lightning numerical simulation and the flexibility of target distribution line system modelling, it is a technical-reasonable solution to combine these two models, namely the hybrid MTL-PEEC model proposed in our previous publications [11, 23]. The hybrid MTL-PEEC model maintains the computational efficiency and accuracy that traditional calculation methods find difficult to solve when dealing with lightning surges in mixed long and short line systems. Additionally, it has great modelling flexibility for large-scale distribution line systems. The specific method introduction, as well as the overhead line modelling and direct lightning risk assessment for the proposed method, can be found in the previous publications [11, 23].

Field LMEP experiments require a significant amount of investment and typically require a long time to obtain reliable results. From 2018 to 2019, rocket triggered lightning induced overvoltage tests were conducted in power distribution lines. Although lightning strike data and overvoltage data under different configurations have been obtained, the experimental observation data is limited, and it is not easy to cover all operating conditions for further research. The hybrid MTL-PEEC method [11, 24] has been validated in the application of direct lightning overvoltage in transmission lines with simple line structures, but has not yet been compared with LEMP observations in complex distribution line systems.

In response to the above issues, in the present study, we adopted the hybrid MTL-PEEC method to calculate the rocket-triggered LEMP on the 10 kV experiment distribution line system based on the real configuration, and compared the calculation results with the results of the artificial lightning triggering test. Then, the hybrid method is adopted to calculate the lightning-induced overvoltage on the double-circuit parallel unequal length line without shield wire and only with lightning surge arresters at the ends of the line. All the considered lines for simulation are the extended configurations based on the rocket-triggered test line. The effects of various factors on the amplitude of overvoltage and pole flashover along the line are discussed. The research results indicate that the hybrid MTL-PEEC method integrates the efficiency and accuracy of numerical calculations well and can be applied to large-scale overhead power lines for calculating induced lightning overvoltage in power lines, providing a theoretical basis for subsequent research on lightning protection measures for power lines.

The structure of this article is organised as follows. Section 2 introduces the proposed MTL-PEEC method. The comparison between the calculation results of the method and the actual rocket-triggered measurement results is discussed in Section 3 to verify the feasibility of the method in LEMP simulation for complex line system. The fourth section presents the results of lightning-induced overvoltage calculated by the MTL-PEEC method, analyses the influence of different factors on the maximum overvoltage value, and provides the statistics and analysis of pole flashover. The final section is the conclusion.

2 | MTL-PEEC Model

2.1 | Lightning Current Waveform and Component Model

Two typical waveforms, that is, the first return-stroke current waveform $i_{st}(t)$ and the subsequent return-stroke current waveform $i_{sb}(t)$ are adopted for lightning LEMP simulation. The first return-stroke current waveform is widely represented by the Heidler function, and the subsequent return-stroke current waveform is represented by the sum of two Heidler functions [25], presented as follows [26]:

$$\begin{cases} i_{st}(t) = \dfrac{I_1}{\eta_1} \cdot \dfrac{(t/\tau_1)^n}{1+(t/\tau_1)^n} \cdot \mathrm{e}^{\left(-\frac{t}{\tau_2}\right)} \\ i_{sb}(t) = \dfrac{I_2}{\eta_2} \cdot \dfrac{(t/\tau_3)^n}{1+(t/\tau_3)^n} \cdot \mathrm{e}^{\left(-\frac{t}{\tau_4}\right)} + \dfrac{I_3}{\eta_3} \cdot \dfrac{(t/\tau_5)^n}{1+(t/\tau_5)^n} \cdot \mathrm{e}^{\left(-\frac{t}{\tau_6}\right)}, \end{cases} \tag{1}$$

where t is time, n is the order that describes the steepness of the current, I_1, I_2 and I_3 is the peak current, η_1, η_2 and η_3 is the correction factor for the amplitude of lightning current, τ_1, τ_3 and τ_5 is the time constant that determines the rise time of the current, and τ_2, τ_4 and τ_6 is the time constant that determines the decay time of the current. Note that the formulae are often used to define the current of the bottom of lightning return-stroke channels.

After modelling the bottom current of the lightning channel, taking into account the delay effect and amplitude attenuation of the return current development, the current at different heights of the lightning return channel is defined as follows:

$$\begin{cases} i_{st}(z,t) = u\left(t - \dfrac{z}{v_f}\right) \cdot P(z) \cdot i_{st}\left(t - \dfrac{z}{v_f}\right) \\ i_{sb}(z,t) = u\left(t - \dfrac{z}{v_f}\right) \cdot P(z) \cdot i_{sb}\left(t - \dfrac{z}{v_f}\right) \end{cases}, \tag{2}$$

where z is the channel height, $u\ (t - z/v_f)$ is the Heaviside function and equals unit for $t \geq z/v_f$ and zero otherwise, $P(z)$ is the height-dependent attenuation factor, v_f is the upward-propagating return-stroke front speed.

The specific current parameter are shown in Table 1 where I_{max} is the waveform amplitude, $t_{10/90}$ is the wave head time, and the typical lightning current waveform is shown in Figure 1. Considering the current distribution in the lightning channel, the Uman's formula [27] is used to calculate the induced electromagnetic field under ideal earth conditions, and then the Cooray Rubinstein formula [28, 29] is used to consider the impact of lossy earth.

TABLE 1 | Parameters of return-stroke current waveform.

	Value		
Parameter	**First return-stroke**	**Subsequent return-stroke**	
I_{1-3} (kA)	$I_1 = 29.3$	$I_2 = 10.7$	$I_3 = 6.5$
n	2	2	2
τ_{1-6} (μs)	$\tau_1 = 1.44$	$\tau_3 = 0.25$	$\tau_5 = 2.5$
	$\tau_2 = 91.8$	$\tau_4 = 2.1$	$\tau_6 = 230$
I_{max} (kA)	31.1	12.3	
$t_{10/90}$ (μs)	2.72	0.38	

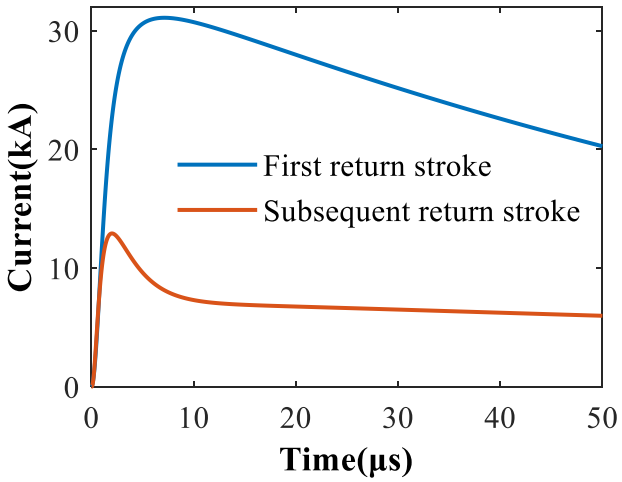

FIGURE 1 | The first and subsequent lightning return-stroke current waveform.

The lightning surge arrester uses the frequency dependent equivalent circuit model recommended by IEEE. In this model, the nonlinear *V–I* (Volt–Ampere) characteristics of the surge arrester are represented by two nonlinear resistors, A_0 and A_1, as shown in Figures 2 and 3. The volt ampere characteristic curve of nonlinear resistors is shown in Figure 3 [30, 31], where V_{10} is the normalised voltage reference value.

The insulator adopts the critical flashover voltage (CFO) model recommended by IEEE [32]. The threshold level is usually assumed to be the line CFO multiplied by a coefficient. The specific value selected as 1.5 times the CFO value is 296 kV.

2.2 | MTL Model

The long horizontal conductors of overhead lines (OHLs) can be modelled using the MTL method. We use the classic Agrawal's field line coupling model [33] to solve the lightning electromagnetic pulse radiated by non-direct lightning strikes on overhead lines. The time-domain coupling equation of Agrawal above the lossy ground is as follows:

$$\begin{aligned} &\frac{\partial}{\partial x}\boldsymbol{v}_i^s(x,t) + \boldsymbol{L}_{ij}\frac{\partial}{\partial t}\boldsymbol{i}_i(x,t) + \boldsymbol{\xi}_{ij}(x,t) \otimes \frac{\partial}{\partial t}\boldsymbol{i}_i(x,t) \\ &\quad = \boldsymbol{E}_x^e(x,h,t)\frac{\partial}{\partial x}\boldsymbol{i}_i(x,t) + \boldsymbol{C}_{ij}\frac{\partial}{\partial t}\boldsymbol{v}_i^s(x,t) \\ &\quad = 0, \end{aligned} \tag{3}$$

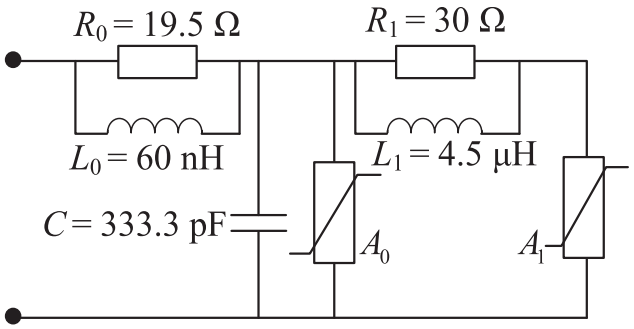

FIGURE 2 | Frequency variation equivalent circuit of surge arrester.

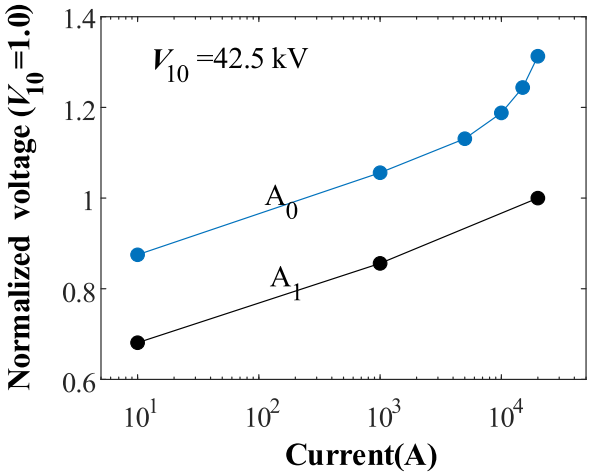

FIGURE 3 | *V–I* characteristic curve of nonlinear resistance.

where $\boldsymbol{i}_i(x, t)$ and $\boldsymbol{v}_i^{\mathrm{s}}(x, t)$ are the lightning-induced current vector and lightning-induced voltage vector on the line, respectively, $\boldsymbol{E}_x^{\mathrm{e}}(x, h, t)$ is the lightning-induced horizontal electric field along the line at the height h of the conductor, $\boldsymbol{\xi}_{ij}(x, x)$ is an approximate transient grounding impedance matrix between the horizontal parallel conductor i and j, where convolution represents the voltage drop along the line caused by lossy ground. For typical overhead lines and lightning frequency ranges, the internal resistance of the conductor can be ignored with reasonable accuracy. $\boldsymbol{L}_{ij}$ and $\boldsymbol{C}_{ij}$ are the unit length inductance and capacitance matrices of multiple conductors [34]:

The boundary equations of the Agrawal model are as follows:

$$\begin{cases} \boldsymbol{V}_i^{\mathrm{s}}(0, \mathrm{t}) = -\boldsymbol{R}_{\mathrm{S}} \cdot \boldsymbol{I}_i(0, t) - \boldsymbol{V}_i^{\mathrm{e}}(0, t) \\ \boldsymbol{V}_i^{\mathrm{s}}(L, \mathrm{t}) = -\boldsymbol{R}_{\mathrm{L}} \cdot \boldsymbol{I}_i(L, t) - \boldsymbol{V}_i^{\mathrm{e}}(L, t) \end{cases}, \tag{4}$$

where $\boldsymbol{R}_{\mathrm{S}}$ and $\boldsymbol{R}_{\mathrm{L}}$ are the resistance matrices of the multiconductor supply and load terminals. $\boldsymbol{V}_i^{\mathrm{e}}(0, t)$ is an equivalent voltage source, mainly determined by the integration along the vertical induced electric field. The total induced voltage vector $\boldsymbol{V}_i(x, t)$ is determined by adding the scattering voltage and the correction term, as follows:

$$\boldsymbol{V}_i(x, t) = \boldsymbol{V}_i^{\mathrm{s}}(x, t) - \int_0^h \boldsymbol{E}_z^{\mathrm{e}}(x, z, t)\mathrm{d}z. \tag{5}$$

2.3 | PEEC Model

Short lines in the distribution system, such as poles, grounding grids, lightning channels, etc., can be equivalent to line structures, which are divided into small segments for PEEC modelling. The PEEC model was initially proposed by A. Ruehli [35, 36] and derived from the mixed potential integral equations (MPLE) of wires. Using the PEEC method in the time domain is more intuitive than analysing transient responses in the frequency domain. The circuit interpretation of the PEEC equation can be derived from the following mixed potential integral equation:

$$\boldsymbol{E}(r, t) = -\frac{\partial \boldsymbol{A}(r, t)}{\partial t} - \nabla \boldsymbol{\Phi}(r, t) + \boldsymbol{E}_{\mathrm{inc}}(r, t), \tag{6}$$

where $\boldsymbol{E}(r, t)$ is the electric field, $\boldsymbol{A}(r, t)$ and $\boldsymbol{\Phi}(r, t)$ is a magnetic vector and a scalar potential, respectively. $\boldsymbol{E}_{\mathrm{inc}}$ is the incident electric field, t is time and r is the position vector. In circuit implementation, MPLE can be further explained as Kirchhoff's voltage law (KVL) and Kirchhoff's current law (KCL), and the corresponding circuit is shown in Figure 4.

The PEEC circuit equation for the ith conductor is described as follows using branch current $\boldsymbol{I}_i$ and node voltage $\boldsymbol{V}_k$:

$$\begin{cases} \boldsymbol{V}_{k+1} - \boldsymbol{V}_k = \boldsymbol{R}_{ii}\boldsymbol{I}_i + \boldsymbol{L}_{ii}\dfrac{\mathrm{d}\boldsymbol{I}_i}{\mathrm{d}t} + \displaystyle\sum_{j\neq i}\boldsymbol{L}_{ij}\frac{\mathrm{d}\boldsymbol{I}_j}{\mathrm{d}t} + \boldsymbol{U}_{\mathrm{s},i} \\ \dfrac{1}{\boldsymbol{p}_{kk}}\dfrac{\mathrm{d}\boldsymbol{V}_k}{\mathrm{d}t} - \displaystyle\sum_{m\neq k}\frac{\boldsymbol{p}_{km}}{\boldsymbol{p}_{mm}}\boldsymbol{I}_{\mathrm{c},j} - \boldsymbol{I}_{\mathrm{s},k} = 0 \end{cases}, \tag{7}$$

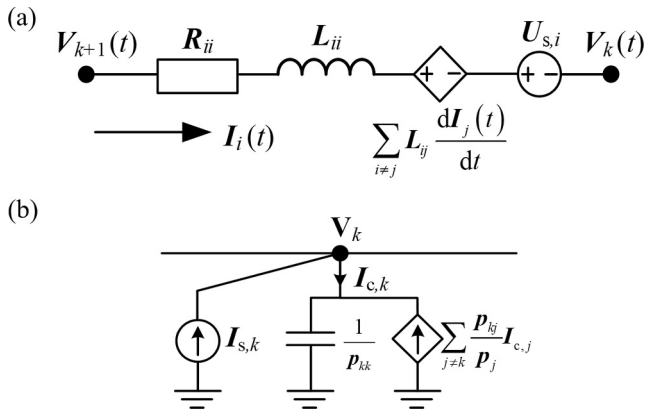

FIGURE 4 | PEEC model circuit diagram for a section of the line. (a) Inductive circuit, (b) capacitive circuit.

where $\boldsymbol{R}_{ii}$ is the segmented resistor, $\boldsymbol{L}_{ii}$ is a segmented inductor, and $\boldsymbol{L}_{km}$ and $\boldsymbol{p}_{km}$ are partial component param of inductance and potential coefficient between section i and section j, or between node k and node m.

In Formula (7) $\boldsymbol{U}_{\mathrm{s},i}$ and $\boldsymbol{I}_{\mathrm{s},k}$ are external voltage sources and external current sources, namely lightning power sources. The circuit explanation of Formula (7) is shown in Figure 4. The capacitance current vector $\boldsymbol{I}_{\mathrm{c},j}$ can be represented by $\boldsymbol{A}^{\mathrm{T}}\boldsymbol{I}_{\mathrm{b},j} + \boldsymbol{I}_{\mathrm{s},j}$, where $\boldsymbol{A}^{\mathrm{T}}$ is the incident matrix of the network, and $\boldsymbol{I}_{\mathrm{b},j}$ and $\boldsymbol{I}_{\mathrm{s},j}$ are the branch current and source current, respectively. When the distance between two-line segments is equivalent to one-tenth of the wavelength, the delay effect in coupling should be considered. Let $\boldsymbol{L}$ and $\boldsymbol{P}$ be the inductance and potential coefficient matrices of the network, as follows:

$$\begin{cases} \boldsymbol{L} = \boldsymbol{L}_{\mathrm{S}} + \boldsymbol{L}_{\mathrm{m}} \\ \boldsymbol{P} = \boldsymbol{P}_{\mathrm{S}} + \boldsymbol{P}_{\mathrm{m}} \end{cases}, \tag{8}$$

where $\boldsymbol{L}_{\mathrm{S}}$ and $\boldsymbol{P}_{\mathrm{S}}$ are full-size matrices, and the elements have no time delay, $\boldsymbol{L}_{\mathrm{m}}$ and $\boldsymbol{P}_{\mathrm{m}}$ are matrices containing the entries for the elements with time delay. The full wave PEEC model established from these matrices is given as follows:

$$\begin{bmatrix} -\boldsymbol{A} & -\boldsymbol{R} - \boldsymbol{L}_{\mathrm{S}}\dfrac{\mathrm{d}}{\mathrm{d}t} \\ \boldsymbol{P}_{\mathrm{S}}^{-1}\dfrac{\mathrm{d}}{\mathrm{d}t} & -\boldsymbol{A}^{\mathrm{T}} \end{bmatrix} \begin{bmatrix} \boldsymbol{V}_{\mathrm{n}}(t) \\ \boldsymbol{I}_{\mathrm{b}}(t) \end{bmatrix} = \begin{bmatrix} \boldsymbol{U}_{\mathrm{S}}(t) + \boldsymbol{L}_{\mathrm{m}}\dfrac{\mathrm{d}}{\mathrm{d}t}\boldsymbol{I}_{\mathrm{b}}(t-\tau) \\ \boldsymbol{I}_{\mathrm{S}}(t) + \boldsymbol{P}_{\mathrm{S}}^{-1}\boldsymbol{P}_{\mathrm{m}}\left(\boldsymbol{A}^{\mathrm{T}}\boldsymbol{I}_{\mathrm{b}}(t-\tau) + \boldsymbol{I}_{\mathrm{S}}(t-\tau)\right) \end{bmatrix}, \tag{9}$$

where $\boldsymbol{R}$ is the impedance matrix. $\boldsymbol{V}_{\mathrm{n}}$ and $\boldsymbol{U}_{\mathrm{S}}$ are voltage sources on nodes and branches, respectively. τ is the delay time between line segments.

2.4 | Backward Euler Synchronous Solution

The backward Euler method is used to simultaneously solve the MTL and PEEC models established above. When both long and short wires exist in the system, mutual coupling can be included

in the system equation. This coupling is modelled using the PEEC method and represented by parameter $\boldsymbol{L}_{\mathrm{m}}$ and $\boldsymbol{P}_{\mathrm{m}}$. The mixed network equation for unknown voltage and current on long and short wires is given as follows:

$$\begin{bmatrix} & & \boldsymbol{L}_{\mathrm{lw}}\dfrac{\mathrm{d}}{\mathrm{d}t} & \boldsymbol{L}_{\mathrm{m,o}} & \\ & -\boldsymbol{A} & & & \\ & & \boldsymbol{L}_{\mathrm{m,o}}^{\mathrm{T}} & -\boldsymbol{R}_{\mathrm{sw}}-\boldsymbol{L}_{\mathrm{sw,o}}\dfrac{\mathrm{d}}{\mathrm{d}t} & \\ \boldsymbol{C}_{\mathrm{lw}}\dfrac{\mathrm{d}}{\mathrm{d}t} & \boldsymbol{P}_{\mathrm{m,o}} & & & \\ & & & -\boldsymbol{A}^{\mathrm{T}} & \\ \boldsymbol{P}_{\mathrm{m,o}}^{\mathrm{T}} & \boldsymbol{P}_{\mathrm{sw,o}}^{-1}\dfrac{\mathrm{d}}{\mathrm{d}t} & & & \end{bmatrix} \begin{bmatrix} \boldsymbol{V}_{\mathrm{lw}}(t) \\ \boldsymbol{V}_{\mathrm{sw}}(t) \\ \boldsymbol{I}_{\mathrm{lw}}(t) \\ \boldsymbol{I}_{\mathrm{sw}}(t) \end{bmatrix} = \begin{bmatrix} \boldsymbol{U}_{\mathrm{lw,s}}(t)+\xi(t)\otimes\boldsymbol{I}_{\mathrm{lw}}(t)+\boldsymbol{L}_{\mathrm{m,d}}\dfrac{\mathrm{d}}{\mathrm{d}t}\boldsymbol{I}_{\mathrm{sw}}(t-\tau) \\ \boldsymbol{U}_{\mathrm{sw,s}}(t)+\boldsymbol{L}_{\mathrm{sw,d}}\dfrac{\mathrm{d}}{\mathrm{d}t}\boldsymbol{I}_{\mathrm{sw}}(t-\tau)+\boldsymbol{L}_{\mathrm{m,d}}^{\mathrm{T}}\dfrac{\mathrm{d}}{\mathrm{d}t}\boldsymbol{I}_{\mathrm{lw}}(t-\tau) \\ \boldsymbol{A}^{\mathrm{T}}\boldsymbol{I}_{\mathrm{lw}}(t)+\boldsymbol{C}_{\mathrm{lw}}\boldsymbol{P}_{\mathrm{m}}\left(\boldsymbol{A}^{\mathrm{T}}\boldsymbol{I}_{\mathrm{sw}}(t-\tau)+\boldsymbol{I}_{\mathrm{sw,s}}(t-\tau)\right) \\ \boldsymbol{I}_{\mathrm{sw,s}}(t)+\boldsymbol{P}_{\mathrm{m,o}}^{-1}\left\{\boldsymbol{P}_{\mathrm{sw,d}}\left[\boldsymbol{A}^{\mathrm{T}}\boldsymbol{I}_{\mathrm{sw}}(t-\tau)+\boldsymbol{I}_{\mathrm{sw,s}}(t-\tau)\right]+\boldsymbol{P}_{\mathrm{m,d}}^{\mathrm{T}}\left[\boldsymbol{A}^{\mathrm{T}}\boldsymbol{I}_{\mathrm{lw}}(t-\tau)+\boldsymbol{I}_{\mathrm{lw,s}}(t-\tau)\right]\right\} \end{bmatrix}. \tag{10}$$

Among them, $\boldsymbol{R}$ is the resistance matrix, $\boldsymbol{L}$ and $\boldsymbol{C}$ are the inductance and capacitance matrices per unit length, respectively, $\boldsymbol{V}(t)$ and $\boldsymbol{I}(t)$ are the node voltage and branch current, respectively, and τ is the delay time between segments. The subscripts $\boldsymbol{U}_{\mathrm{S}}$ and $\boldsymbol{I}_{\mathrm{S}}$ represent the voltage source and current source, respectively. The subscript of 'lw' represents the param of a long wire. The subscript of 'sw' represents the param of the short wire. The subscript 'o' describes matrix retention entries without time delay, and 'd' represents those with time delay. The backward Euler method is used to solve the equation. The voltage and current in the entire system are updated simultaneously, that is, in $n{\cdot}\mathrm{d}t$ steps.

3 | Model Validation

3.1 | Rocket Induced Lightning Experiment

At present, research on lightning overvoltage in distribution lines can be divided into natural lightning observation tests, rocket induced lightning tests, artificial injection impulse tests, scaled model tests and numerical simulations. Rocket induced lightning technology can be used for artificial lightning, thus playing an important role in lightning physics research [37]. The beginning of artificial lightning triggering technology was in 1967 when Newman and others successfully triggered 17 events from thunderstorms to ships [38]. The research on distribution lines using rocket induced lightning mainly focuses on the current diversion along the line and the measurement of line overvoltage [39].

Based on a typical 10 kV distribution line, the double circuit 10 kV test line was completed in 2018, located at the junction of mountainous and plain areas in Conghua City, Guangdong Province, China, which is prone to thunderstorms [40]. There are a total of 22 poles in the distribution line, with a spacing of approximately 70 m between each pole. The first 17 poles are of double circuit structure, whereas poles 18–22 are of single circuit structure. The length of the line between poles 1–17 is 1122 m, and the total length of the line between poles 18–22 is 391 m. Due to geographical limitations, the circuit I route is L-shaped, running from pole 1 to pole 22. The circuit II line runs from pole 1 to pole 17. The horizontal interval between circuit I and circuit II is 2.5 m as shown in Figure 5. The three-phase wires of the experimental circuit are arranged vertically. Phase C is at the bottom, with a height of 10 m from the ground, and the spacing between phase conductors is about 0.9 m. The ground wire is located 1 m above phase A of circuit I. The soil resistivity range is 180–200 Ω·m. The range of pole impact grounding resistance values is 8–26 Ω.

In the experiment, a shield wire is installed 1 m above the circuit I line, and is grounded at individual poles one by one. The surge arresters are installed at the beginning and end of circuit I. The insulator model is S-210, with a 50% impulse discharge voltage of about 240 kV for positive polarity and 296 kV for negative polarity. The lightning strike point is 40 m away from the line, as shown in Figure 6.

3.2 | Experimental and Simulation Waveforms

The rocket induced lightning test was conducted in Conghua, Guangdong, China at 15:22 on June 5, 2019. A lightning event, numbered F1906051522 and containing two return strokes, was recorded on pole 14 along the circuit I line. The range of soil resistivity is 180–200 Ω·m.

The voltage waveforms corresponding to two return-strokes is recorded. The lightning current waveform obtained from the experiment is shown in Figure 7, where RS1 is the first return-stroke and RS2 is the second return-stroke. The current amplitude of the first return-stroke is 30.83 kA, with a rise time $t_{10/90}$ of 0.12 μs and the time to half wave $t_{50/50}$ of 7.24 μs. The current amplitude of the second return stroke is 29.00 kA, with a rise time $t_{10/90}$ of 0.06 μs and the time to half wave $t_{50/50}$ of 1.74 μs.

Based on existing line and equipment parameter, the proposed MTL-PEEC hybrid method is adopted to calculate the lightning-induced overvoltage waveform on pole 14 of the circuit I lines for comparison with the test measurement. The comparison between the test voltage waveform and the simulated voltage waveform is shown in Figure 8 and Table 2.

As shown in Figure 8, in order to better distinguish each waveform, some waveforms have been artificially increased in offset. It can be seen that the simulation results are basically

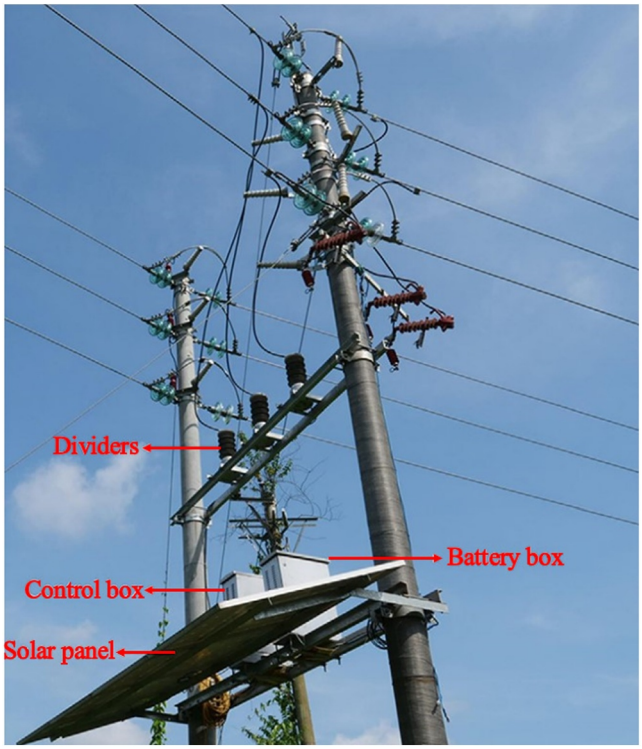

FIGURE 5 | Overvoltage observation system.

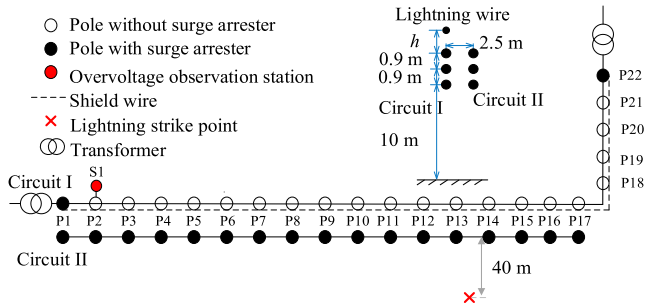

FIGURE 6 | The topology of the distribution line for rocket-triggered.

consistent with the test results. This indicates that the MTL-PEEC hybrid analysis method can be used to simulate the waveform of lightning-induced overvoltage. Additionally, this method also has good effects on simulating lightning waveforms with short wavefront time and half wave time.

Note that the initial reverse polarity pulse before the first overvoltage peak is related to the step-leader process, which have not been reflected in the lightning channel model for calculation. This would be further studied for the improvement of the full-electromagnetic effect consideration.

4 | Lemp Study on Different Lightning Positions, Amplitudes and Tower Grounding Resistance

This section focuses on studying the LEMP effect of different lightning current waveforms, lightning current amplitudes, grounding conditions and lightning strike points on overhead distribution lines without using lightning arresters and shielding wires.

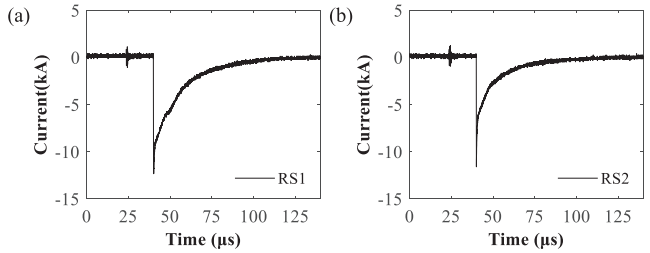

FIGURE 7 | Triggered lightning current waveform for RS1 and RS2. (a) RS1 lightning current waveform, (b) RS2 lightning current waveform.

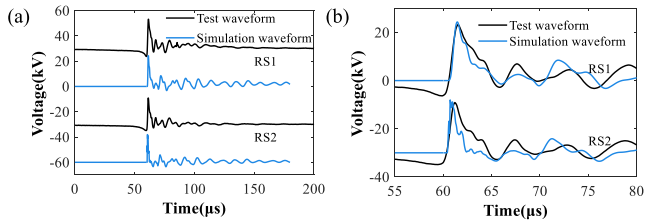

FIGURE 8 | Comparison of tested waveform and simulation waveform. (a) Tested waveform and simulation waveform, (b) comparison of tested waveform and simulation waveform.

TABLE 2 | Summary table of calculated variables.

	RS1		RS2	
Variable	**Test**	**Simulation**	**Test**	**Simulation**
Amplitude (kV)	23.20	24.33	20.88	21.95
$t_{10/90}$ (μs)	0.61	0.47	0.55	0.24
$t_{50/50}$ (μs)	2.34	1.52	1.50	0.82

4.1 | Simulation Conditions

In the present study, 10 kV double circuit parallel unequal length lines is selected for calculation and analysis, the diagram of which are shown in Figure 9. Circuit I of the double circuit line is L-type, with a length of 1500 m, and the circuit II line is linear, with a length of 1100 m. Transformers are installed at both ends of the circuit I line of the double circuit line without shield wire, as shown in Figure 9. The soil conductivity is 0.005 S/m.

Numerical simulations for different lightning current waveforms, amplitudes, grounding resistance and different lightning strike points are conducted, with the simulation conditions shown in Table 3. Specifically, two lightning current waveforms, five lightning current amplitudes and five grounding parameters are considered. The lightning strike points are located in front of pole 9, 560 m away from the leftmost end of the line.

4.2 | Lightning-Induced Overvoltage Waveform on the Pole

Under a typical first return-stroke current waveform, when the lightning strike point is 100 m away from the line and the

grounding resistance is 10 Ω, the three-phase lightning-induced overvoltage waveform on the 9th and 10th pole is shown in Figure 10, and the lightning-induced overvoltage waveform of A-phase on each pole of circuit I are shown in Figure 11.

It is found that the voltage waveforms on the poles exhibiting negative polarity oscillation characteristics, with a negative peak amplitude of phase A voltage of around 140 kV as shown in Figure 11. The amplitude of phase B and phase C voltage is around 130 kV, showing an obvious relative amplitude ordering of phase A > phase B > phase C.

Figure 11 shows the lightning-induced overvoltage waveform of A-phase on each pole of circuit I. It is found that from pole 9 to pole 1, and from pole 10 to pole 21, the voltage amplitude along the line is decreasing. The lightning-induced overvoltage waveform exhibits a characteristic of apparent oscillation with an oscillation period of about 10 μs. Assuming that the wave propagates at the speed of light, with a propagation distance of 3000 m, which is nearly twice the total length of circuit I of 1470 m, this indicates that the oscillation originates from line reflection.

When changing the amplitude of lightning current, lightning strike point, and lightning current waveform, the voltage propagation characteristics of the pole 2 to pole 9 along circuit I are shown in Figure 12. Compared with Figure 11, when the lightning strike point is closer to the line and the lightning current amplitude is larger, the overvoltage waveform develops towards bipolar waveform, but the main peak is still negative polarity.

Figure 13 shows the three negative peak values of the three-phase insulators of pole 2 to pole 21 along the line, under a typical first return-stroke current waveform, with the lightning strike point of 100 m away from the line and the grounding resistance of 10 Ω.

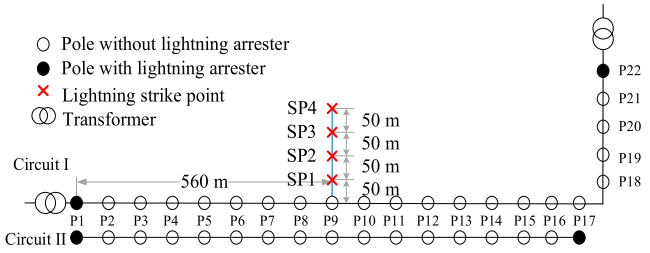

FIGURE 9 | The topology of the extended distribution lines of double circuit parallel unequal length lines for LEMP simulation.

TABLE 3 | Summary table of calculated variables.

Variable	Value				
Lightning current waveform	First return-stroke			Subsequent return-stroke	
Distance between lightning strike point and line (m)	50	100	150	200	
Lightning current amplitude (kA)	10	30	50	80	100
Grounding resistance (Ω)	5	15	25	35	50

It is found that the overvoltage amplitude of phase-C and is always lower than that of phase-A, with a general proportion of about 90%, which would change to some degree under different pole locations or the distance away from the nearest pole 9 from the lightning strike point as shown in Figure 13.

4.3 | Lightning-Induced Overvoltage Amplitude Under Different Lightning Strike Point

The impact of lightning strike point on the voltage amplitude along the line is shown in Figure 14. It is found that the voltage amplitude gradually decays towards both ends of the line centred around pole 9, which is closest to the lightning strike point. The voltage amplitude of pole 9 exceeds 150 kV when lightning strikes SP1. When the lightning strike point is 200 m away from the line, the voltage amplitude of pole 9 is less than 100 kV. Under four types of lightning strikes, namely at a distance of 50, 100, 150 and 200 m directly in front of pole 9 on circuit I line, the voltage amplitude of the terminal pole of the line drops below 50 kV.

4.4 | Lightning-Induced Overvoltage Amplitude Under Different Lightning Current Amplitude

The influence of lightning current amplitude on the maximum lightning-induced overvoltage along circuit I is shown in Figure 15. The solid line represents the first return stroke, and the dashed line represents the subsequent return stroke.

It is found that as the amplitude of the lightning current increases, the maximum lightning-induced overvoltage amplitude

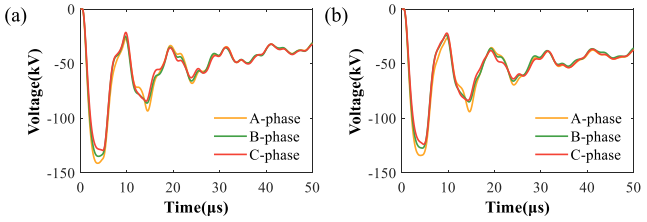

FIGURE 10 | The three-phase overvoltage waveforms on pole 9 and pole 10, under the condition of a typical first return-stroke waveform with a lightning strike point of SP2 and a grounding resistance of 10 Ω. (a) Pole 9, (b) pole 10.

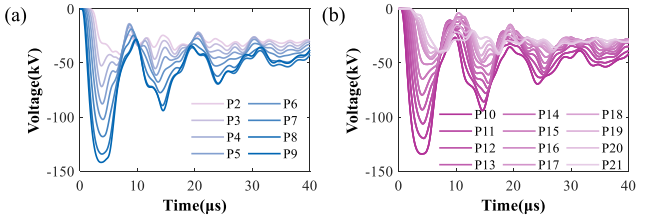

FIGURE 11 | The overvoltage waveform of A-phase on each pole of the circuit I, under the condition of a typical first return-stroke waveform with a lightning strike point of SP2 and a grounding resistance of 10 Ω. (a) Left side of lightning strike point, (b) right side of lightning strike point.

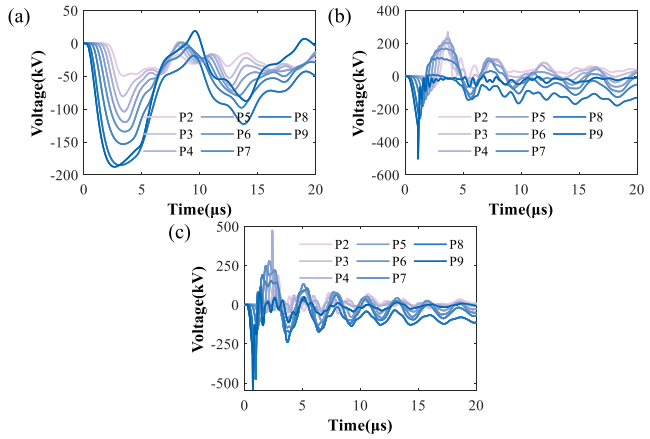

FIGURE 12 | The overvoltage waveform of phase A on each pole of circuit I under different conditions. (a) Typical first return stroke-SP1, (b) first return stroke-SP1-100 kA, (c) subsequent return stroke-SP1-100 kA.

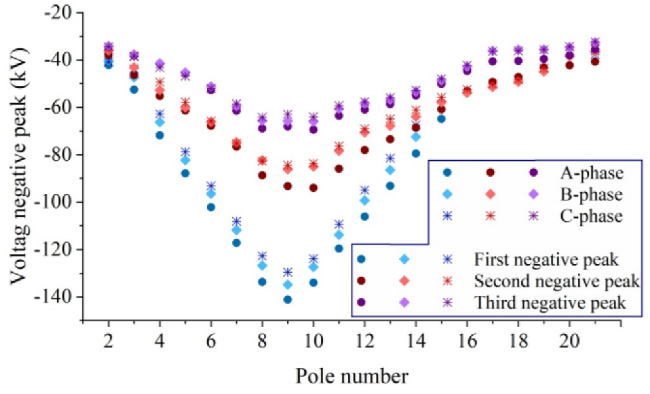

FIGURE 13 | Statistics diagram of negative peak amplitude of pole voltage along circuit I.

along the line increases. On the other hand, the maximum lightning-induced overvoltage amplitude caused by the subsequent return current waveform is always greater than the maximum lightning-induced overvoltage amplitude caused by the first return current waveform. This is because the wavefront time of the subsequent return current waveform is shorter. Moreover, when the lightning current is 50 kA, the lightning strike point SP1 causes flashover. When the amplitude of the lightning current reaches 80 kA, both lightning strike points SP2 and SP3 will cause flashover. As for the case of lightning current reaching 100 kA, four lightning strike points and two types of lightning current waveforms will cause flashover. Note that the larger the lightning current and the closer the lightning strike point is to the line, the more obvious the positive peak value of the voltage waveform.

4.5 | Lightning-Induced Overvoltage Amplitude Under Different Grounding Resistance

Figure 16 reflects the influence of ground resistance on the amplitude of lightning induced overvoltage during the first return-stroke and subsequent return-stroke.

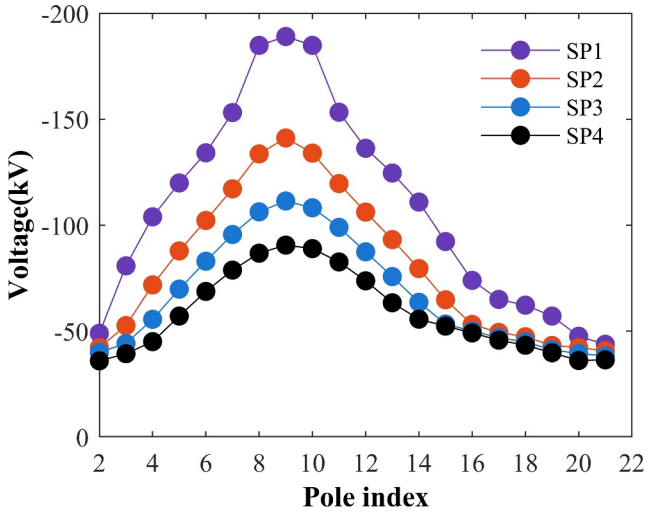

FIGURE 14 | The amplitude of the overvoltage waveform at each pole with different lightning strike points, under a typical first return-stroke current waveform, when the grounding resistance is 10 Ω.

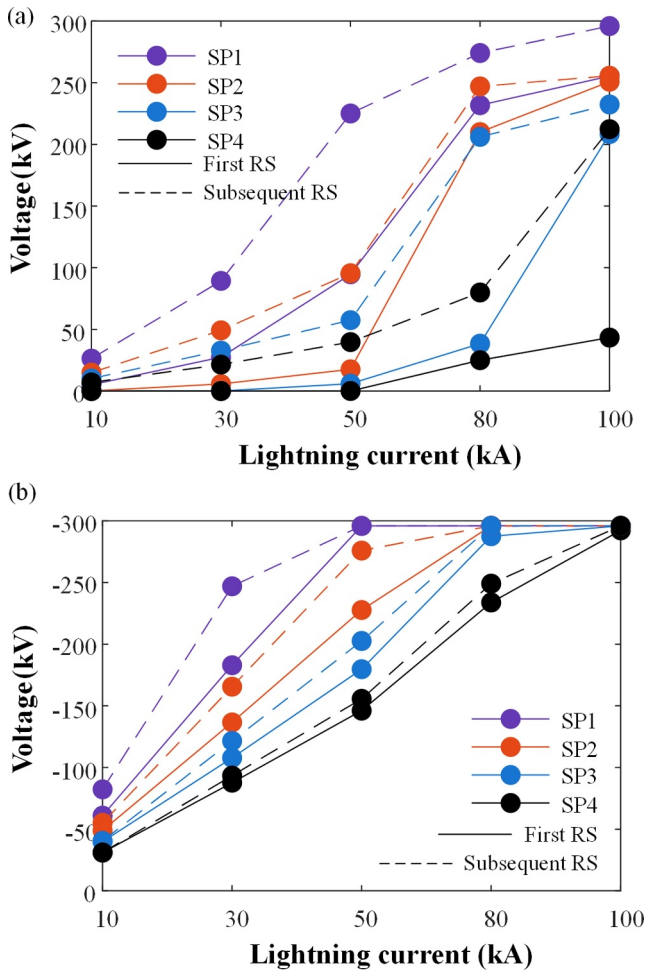

FIGURE 15 | The amplitude of lightning-induced overvoltage of double-circuit lines versus lightning current amplitudes, under different lightning current waveforms, lightning strike points, with a grounding resistance of 10 Ω. (a) Positive amplitude, (b) negative amplitude.

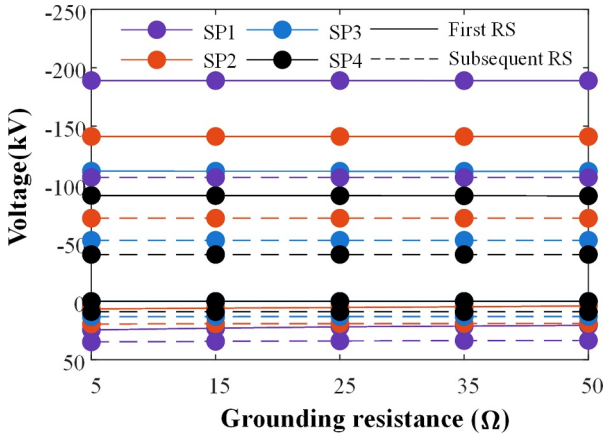

FIGURE 16 | The amplitude of lightning-induced overvoltage of double-circuit lines versus different grounding resistance, under different lightning current waveforms and lightning strike points, with a typical lightning current waveform shown in Figure 1.

It can be seen that the amplitude of the maximum overvoltage peak along the line remains unchanged when the grounding resistance ranges from 5 to 50 Ω with a fixed soil conductivity. Due to the fact that the amplitude of the typical first return current is greater than that of the typical subsequent return current, the maximum lightning-induced voltage along the line caused by it is always higher. The maximum lightning-induced voltage amplitude generated by lightning SP1 on the circuit I line is less than 200 kV.

4.6 | Flashover Situation of Tower Insulators

The flashover voltage of the tower insulator is 197 kV. For lightning strike points 1 and 2 during the first return strike, the A-phase of tower 9 closest to the lightning strike point will flashover after the lightning current exceeds 50 kA. When the lightning strike point is 150 m away from the circuit I line, the lightning current amplitude reaching 100 kA will cause flashover of pole 9. When the lightning strike point is 200 m away from the line, a lightning current of 100 kA will not cause flashover of the circuit I line. For subsequent return-stroke and strike point 50 m away from the line, when the lightning current amplitude is 50 and 80 kA, the A-phase of pole 9 flashes. When the amplitude of lightning current increases to 100 kA, in addition to the 8th, 9th and 10th poles that are very close to the lightning strike point, the 4th and 14th poles also flashover.

5 | Conclusion

In this study, a numerical MTL-PEEC hybrid method proposed in our previous studies is validated by the rocket-triggered lightning experimental results under a more complex line configuration. The agreement between experimental and simulation results further validates the adaptability and accuracy of the proposed method, which is then adopted to calculate the lightning-induced overvoltage on the double-circuit parallel unequal length line without shield wire and only with lightning surge arresters at the ends of the line. All the considered lines for simulation are the extended configurations based on the rocket-triggered test line. The effects of various factors on the amplitude of overvoltage and pole flashover along the line are discussed, with the following conclusions obtained:

For the double circuit line, when lightning strikes the ground in front of the centre of circuit I, the three-phase voltage waveform is similar, both of which are negative or bipolar oscillation waves. The closer the lightning strike point is to the line, the voltage waveform develops towards bipolar waveform, but the main peak remains negative.

As the amplitude of lightning current increases, the maximum lightning-induced voltage amplitude along the line increases, and the maximum lightning-induced voltage amplitude caused by the subsequent return current waveform is always greater than the maximum lightning-induced voltage amplitude caused by the first return current waveform. When the grounding resistance increases from 5 to 50 Ω, the maximum voltage peak amplitude along the line remains unchanged.

Funding

The work is supported by National Natural Science Foundation of China (No. 52507193).

Conflicts of Interest

The authors declare no conflicts of interest.

Data Availability Statement

The data that support the findings of this study are available from the corresponding author upon reasonable request.

References

1. F. Rachidi, C. A. Nucci, M. Ianoz, and C. Mazzetti, "Response of Multiconductor Power Lines to Nearby Lightning Return Stroke Electromagnetic Fields," *IEEE Transactions on Power Delivery* 12, no. 3 (1997): 1404–1411.

2. J. Takami, T. Tsuboi, K. Yamamoto, S. Okabe, and Y. Baba, "Lightning Surge Characteristics on Inclined Incoming Line to Substation Based on Reduced-Scale Model Experiment," *IEEE Transactions on Dielectrics and Electrical Insulation* 20, no. 3 (2013): 739–746.

3. A. J. Eriksson and D. V. Meal, "Lightning Performance and Overvoltage Surge Studies on a Rural Distribution Line," *IEE Proceedings - Part C: Generation, Transmission & Distribution* 129, no. 2 (1982): 59–69.

4. X. Wen, X. Peng, and G. Xie, "Numerical Calculation of Induced Lightning Overvoltage in Overhead Distribution Lines," *Journal of Chinese Electrical Engineering Science* 18, no. 4 (1998): 76–78 (in Chinese).

5. R. Zeng, C. Zhuang, X. Zhou, et al., "Survey of Recent Progress on Lightning and Lightning Protection Research," *High Voltage* 1, no. 1 (2016): 2–10.

6. S. Yokoyama, "Calculation of Lightning-Induced Voltages on Overhead Multiconductor Systems," *IEEE Transactions on Power Apparatus and Systems* PAS-103, no. 1 (1984): 100–108.

7. T. E. McDermott, T. A. Short, and J. G. Anderson, "Lightning Protection of Distribution Lines," *IEEE Transactions on Power Delivery* 9, no. 1 (1994): 138–152.

8. M. Paolone, C. A. Nucci, E. Petrache, and F. Rachidi, "Mitigation of Lightning-Induced Overvoltages in Medium Voltage Distribution Lines by Means of Periodical Grounding of Shielding Wires and of Surge Arresters: Modeling and Experimental Validation," *IEEE Transactions on Power Delivery* 19, no. 1 (2004): 423–431.

9. N. Y. Ahmed, H. A. Illias, and H. Mokhlis, "A Protocol for Selecting Viable Transmission Line Arrester for Optimal Lightning Protection," *Electric Power Systems Research* 221 (2023): 109489.

10. N. Y. Ahmed, H. A. Illias, H. Mokhlis, D. Fahmi, and N. Abdullah, "Flashover Pattern Analysis for 275 kV Double Circuit Transmission Lines During Direct Lightning Strikes," *Electric Power Systems Research* 228 (2024): 110104.

11. J. Cao, Y. Du, Y. Ding, et al., "Lightning Surge Analysis of Transmission Line Towers With a Hybrid FDTD-PEEC Method," *IEEE Transactions on Power Delivery* 37, no. 2 (2022): 1275–1284.

12. K. Ishimoto, F. Tossani, F. Napolitano, A. Borghetti, and C. A. Nucci, "Direct Lightning Performance of Distribution Lines With Shield Wire Considering LEMP Effect," *IEEE Transactions on Power Delivery* 37, no. 1 (2022): 76–84.

13. P. Duan, L. Zhang, X. Huang, J. Sun, Y. Qi, and Q. Yang, "Evaluation of Lightning-Induced Overvoltage on a 10 kV Distribution Line Based on Electromagnetic Return-Stroke Model Using Finite-Difference Time-Domain," *High Voltage* 9, no. 2 (2024): 356–366.

14. Li Cai, Y. Du, W. Fan, et al., "Differences in M-Components Between Triggered Lightning Striking the Ground and Overhead Line," *High Voltage* 9, no. 6 (2024): 1260–1269.

15. C. A. Nucci, F. Rachidi, M. V. Ianoz, and C. Mazzetti, "Lightning-Induced Voltages on Overhead Lines," *IEEE Transactions on Electromagnetic Compatibility* 35, no. 1 (1993): 75–86.

16. G. Diendorfer and M. A. Uman, "An Improved Return Stroke Model With Specified Channel-Base Current," *Journal of Geophysical Research: Atmospheres* 95, no. D9 (1990): 13621–13644.

17. A. Tatematsu and T. Ueda, "FDTD-Based Lightning Surge Simulation of an HV Air-Insulated Substation With Back-Flashover Phenomena," *IEEE Transactions on Electromagnetic Compatibility* 58, no. 5 (2016): 1549–1560.

18. C. A. Nucci, F. Rachidi, M. Ianoz, and C. Mazzetti, "Comparison of Two Coupling Models for Lightning-Induced Overvoltage Calculations," *IEEE Transactions on Power Delivery* 10, no. 1 (1995): 330–339.

19. A. E. A. Araujo, J. O. S. Paulino, J. P. Silva, and H. W. Dommel, "Calculation of Lightning-Induced Voltages With Rusck's Method in EMTP: Part I: Comparison With Measurements and Agrawal's Coupling Model," *Electric Power Systems Research* 60, no. 1 (2001): 49–54.

20. F. Rachidi, M. Rubinstein, S. Guerrieri, and C. A. Nucci, "Voltages Induced on Overhead Lines by Dart Leaders and Subsequent Return Strokes in Natural and Rocket-Triggered Lightning," *IEEE Transactions on Electromagnetic Compatibility* 39, no. 2 (1997): 160–166.

21. R. Qi, Y. P. Du, and M. Chen, "A Full-Wave PEEC Model of Thin-Wire Structures Above the Lossy Ground," *IEEE Transactions on Electromagnetic Compatibility* 62, no. 5 (2020): 2055–2064.

22. I. Hetita, D. E. A. Mansour, Y. Han, et al., "Evaluating Transient Behaviour of Large-Scale Photovoltaic Systems During Lightning Events Using Enhanced Finite Difference Time Domain Method With Variable Cell Size Approach," *High Voltage* 9, no. 3 (2024): 636–647.

23. J. Cao, Y. Ding, Y. Du, M. Chen, and R. Qi, "Design Consideration of the Shielding Wire in 10 kV Overhead Distribution Lines Against Lightning-Induced Overvoltage," *IEEE Transactions on Power Delivery* 36, no. 5 (2021): 3005–3013.

24. F. Qiu, J. Cao, Y. Ding, Y. Du, and Z. Du, "Simulation of Ground Potential Distribution Around Grounding Grids Using a PEEC Method," in *Proc. 2022 IEEE/IAS 58th Industrial and Commercial Power Systems Technical Conference (I&CPS)* (2022), 1–5.

25. F. Tossani, F. Napolitano, A. Borghetti, et al., "Influence of the Presence of Grounded Wires on the Lightning Performance of a Medium-Voltage Line," *Electric Power Systems Research* 196 (2021): 107206.

26. F. Heidler and J. Cvetić, "A Class of Analytical Functions to Study the Lightning Effects Associated With the Current Front," *European Transactions on Electrical Power* 12, no. 2 (2002): 141–150.

27. M. A. Uman, D. Kenneth McLain, and E. Philip Krider, "The Electromagnetic Radiation From a Finite Antenna," *American Journal of Physics* 43, no. 1 (1975): 33–38.

28. V. Cooray, "Horizontal Fields Generated by Return Strokes," *Radio Science* 27, no. 4 (1992): 529–537.

29. M. Rubinstein, "An Approximate Formula for the Calculation of the Horizontal Electric Field From Lightning at Close, Intermediate, and Long Range," *IEEE Transactions on Electromagnetic Compatibility* 38, no. 3 (1996): 531–535.

30. IEEE Working Group 3.4.11, Application of Surge Protective Devices Subcommittee, and Surge Protective Devices Committee, "Modeling of Metal Oxide Surge Arresters," *IEEE Transactions on Power Delivery* 7, no. 1 (1992): 302–309.

31. J. A. Martinez and D. W. Durbak, "Parameter Determination for Modeling Systems Transients-Part V: Surge Arresters," *IEEE Transactions on Power Delivery* 20, no. 3 (2005): 2073–2078.

32. IEEE, "IEEE Guide for Improving the Lightning Performance of Electric Power Overhead Distribution Lines," in *IEEE Std 1410-2004* (IEEE, 2004).

33. A. K. Agrawal, H. J. Price, and S. H. Gurbaxani, "Transient Response of Multiconductor Transmission Lines Excited by a Nonuniform Electromagnetic Field," *IEEE Transactions on Electromagnetic Compatibility* EMC-22, no. 2 (1980): 119–129.

34. A. K. Bhattacharyya, "EMC Analysis Methods and Computational Models," *IEEE Antennas and Propagation Magazine* 39, no. 6 (1997): 68–70.

35. A. Ruehli, U. Miekkala, A. Bellen, and H. Heeb, "Stable Time Domain Solutions for EMC Problems Using PEEC Circuit Models," in *Proceedings of IEEE Symposium on Electromagnetic Compatibility* (1994), 371–376.

36. A. Ruehli, "Partial Element Equivalent Circuit (PEEC) Method and Its Application in the Frequency and Time Domain," in *Proceedings of Symposium on Electromagnetic Compatibility* (1996), 128–133.

37. D. Wang, V. A. Rakov, M. A. Uman, et al., "Characterization of the Initial Stage of Negative Rocket-Triggered Lightning," *Journal of Geophysical Research: Atmospheres* 104, no. D4 (1999): 4213–4222.

38. M. M. Newman, J. R. Stahmann, J. D. Robb, E. A. Lewis, S. G. Martin, and S. V. Zinn, "Triggered Lightning Strokes at Very Close Range," *Journal of Geophysical Research* 72, no. 18 (1967): 4761–4764.

39. M. Rubinstein, M. A. Uman, P. J. Medelius, and E. M. Thomson, "Measurements of the Voltage Induced on an Overhead Power Line 20 m From Triggered Lightning," *IEEE Transactions on Electromagnetic Compatibility* 36, no. 2 (1994): 134–140.

40. J. Wang, Y. Zhao, Li Cai, et al., "Three-Phase Overvoltage at Lightning Strike Point due to Direct Triggered Lightning to the Phase Wire of 10 kV Power Distribution Line," *IET Generation, Transmission & Distribution* 16, no. 11 (2022): 2188–2197.